AD-A193 825 HIGH ENERGY AND HIGH INTENSITY LASER EFFECTS ON AEROSOLS: CHANGES IN DROP..(U) YALE UNIV NEW HAVEN CONN R K CHANG MAR 88 ARO-22517.21-GS DAAG29-85-K-0063 1/1

UNCLASSIFIED F/G 7/3 NL

END
DATE FILMED
7 8

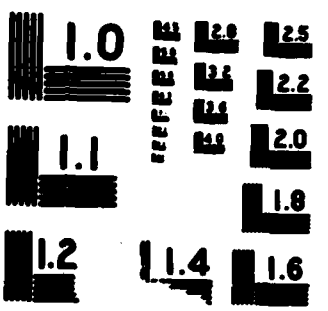
1.0
1.1
1.2
1.4
1.6
1.8
2.0
2.2
2.5

ARO 22517.21-GS
(2)

Final Report

to the

U. S. Army Research Office

High Energy and High Intensity Laser Effects on Aerosols: Changes in Droplet Morphology, Surrounding Temperature, and Vapor Concentration

Contract No: DAAG29-85-K-0063

February 1, 1985 - January 31, 1988

Richard K. Chang
Principal Investigator

Yale University
Section of Applied Physics and Center for Laser Diagnostics
New Haven, Connecticut 06520

March, 1988

UNCLASSIFIED
SECURITY CLASSIFICATION OF THIS PAGE (When Data Entered)

ADA193825

REPORT DOCUMENTATION PAGE

READ INSTRUCTIONS BEFORE COMPLETING FORM

1. REPORT NUMBER: ARO 22517.21-GS	2. GOVT ACCESSION NO.: NA
3. RECIPIENT'S CATALOG NUMBER: NA	
4. TITLE (and Subtitle): HIGH ENERY AND HIGH INTENSITY LASER EFFECTS ON AEROSOLS: CHANGES IN DROPLET MORPHOLOGY, SURROUNDING TEMPERATURE, AND VAPOR CONCENTRATION (Unclassified)	5. TYPE OF REPORT & PERIOD COVERED: FINAL REPORT 2/1/85 - 1/31/88
	6. PERFORMING ORG. REPORT NUMBER
7. AUTHOR(s): Richard K. Chang	8. CONTRACT OR GRANT NUMBER(s): DAAG29-85-K-0063
9. PERFORMING ORGANIZATION NAME AND ADDRESS: Yale University, New Haven, CT 06520	10. PROGRAM ELEMENT, PROJECT, TASK AREA & WORK UNIT NUMBERS: NA
11. CONTROLLING OFFICE NAME AND ADDRESS: U. S. Army Research Office, P. O. Box 12211, Research Triangle Park, NC 27709-2211	12. REPORT DATE: March 1988
	13. NUMBER OF PAGES: 15
14. MONITORING AGENCY NAME & ADDRESS(if different from Controlling Office)	15. SECURITY CLASS. (of this report): UNCLASSIFIED
	15a. DECLASSIFICATION/DOWNGRADING SCHEDULE

16. DISTRIBUTION STATEMENT (of this Report)

Approved for public release; distribution unlimited.

17. DISTRIBUTION STATEMENT (of the abstract entered in Block 20, if different from Report)

NA

18. SUPPLEMENTARY NOTES

The view, opinions and/or findings contained in this report are those of the author(s) and should not be construed as an official Department of the Army position, policy, or decision, unless so designated by other documentation.

19. KEY WORDS (Continue on reverse side if necessary and identify by block number)

Nonlinear optics	Stimulated Raman scattering
Morphology-dependent resonances	Plasma spectroscopy
Laser-induced breakdown	Explosive vaporization
Liquid droplets	Interacting fibers

20. ABSTRACT (Continue on reverse side if necessary and identify by block number)

A summary is presented of our research progress in the area of high intensity and high energy laser interactions with single droplets with radius in the micrometer range. Our main results are related to nonlinear optical effects, which leave the droplet shape intact, and to laser-induced breakdown (LIB) and explosive vaporization, which destroy the droplet.

(Continued)

DD FORM 1 JAN 73 1473 EDITION OF 1 NOV 65 IS OBSOLETE

UNCLASSIFIED
SECURITY CLASSIFICATION OF THIS PAGE (When Data Entered)

20. ABSTRACT CONTINUED

Nonlinear optical interactions in a droplet occur at remarkably low input intensity levels because the droplet acts as a lens to concentrate the input radiation at a location just within the shadow face and as an optical cavity to provide feedback for the internally generated radiation. The following nonlinear optical effects have been observed in single liquid droplets: (1) lasing; (2) stimulated Raman scattering up to the 14th order; (3) coherent Raman gain due to the presence of another input wave; and (4) phase-modulation broadening of the elastically scattered and stimulated Raman scattered radiation.

LIB within the droplet occurs when the rising portion of the input laser pulse causes multiphoton ionization which is followed by cascade multiplication. The resultant plasma within the droplet transforms a nominally transparent droplet into an absorbing droplet, and the remaining portion of the input laser pulse heats the droplet. Plasma is ejected from the droplet, first from the shadow face and then from the illuminated face. Even after the plasma has been quenched, the droplet undergoes explosive vaporization. We have measured the following properties of LIB and explosive vaporization: (1) the location of LIB initiation; (2) the propagation velocities of the ejected plasma; (3) the time-averaged electron density along a line; (4) the time-averaged atomic temperature along a line; and (5) the shape of the droplet as it undergoes explosive vaporization.

Multiple scattering calculations and measurements were made from two closely spaced fibers which served as a prototype of densely packed aerosols. To simplify the experimental requirements, a fiber-mirror configuration was used to approximate the two-fiber configuration. When the fiber-mirror separation was less than the fiber diameter, both interference and interacting effects between the real fiber and its image were observed. The comparison between the exact calculation for two fibers and the experimental results from the fiber-mirror configuration was excellent and provided new insight into the multiple scattering from closely spaced aerosols.

CONTENTS

INTRODUCTION

During the three years of ARO support, significant progress has been made toward furthering the understanding of high energy and high intensity laser beam interactions with single liquid droplets with radius, a, much larger than the incident laser wavelength, λ_0, i.e., droplets with large size parameters $X = 2\pi a/\lambda_0$. Our research efforts involved nonlinear optical effects, such as lasing and four-wave mixing processes, and laser-induced breakdown (LIB) and explosive vaporization effects that occur during and after the laser pulse. In addition, our investigations involved the area of multiple scattering from two closely spaced fibers.

Our research capabilities during the last year were greatly improved by the acquisition of several items of capital equipment through the DoD-University Research Instrumentation Program. In particular, a streak camera enabled us to determine the LIB-generated plasma propagation velocity, and a framing camera allowed us to photograph the droplet during and after explosive vaporization.

RESEARCH ACCOMPLISHMENTS

A brief summary is presented of our main findings related to nonlinear optical effects which leave the droplet shape intact and to LIB and explosive vaporization which dramatically alter the shape of the droplet. The multiple scattering calculations and measurements from two closely spaced fibers which served as a prototype of densely packed aerosols are also described. Details of our accomplishments can be found in the publications resulting from the research (see page 11).

Nonlinear Optical Effects

When a plane wave is incident on a droplet with a large X, the droplet can be envisioned as a lens to concentrate the laser radiation in three places: (1) outside the shadow face, (2) just inside the shadow face, and (3) just inside the illuminated face. While these three locations can be qualitatively predicted by geometric optics, the exact amount of intensity enhancement in the locations requires detailed Lorenz-Mie calculations. Complete knowledge of these high intensity regions is important to all nonlinear optical and LIB studies. Our collaboration with Prof. Peter W. Barber's group at Clarkson University resulted in computer-intensive calculations of the internal- and near-field intensity distribution of a large X sphere and in an experimental mapping of these three locations of intensity concentration by a fluorescence technique (see publication #1).

Another unique feature of a large X droplet is that its spherical liquid-air interface is capable of trapping some of the internally generated radiation (e.g., fluorescence or spontaneous Raman) when the wavelength is equal to one of the numerous wavelengths which correspond to morphology-dependent resonances (MDR's). With geometrics optics, it is known that internal rays which strike the liquid-air interface with angles larger than the critical angle experience quasi-total internal reflection. Using a physical optics description, those internal rays which maintain the same phase front after completing one trip around the entire droplet circumference are trapped within the spherical interface. The droplet for specific wavelengths acts as an optical cavity to provide feedback for the internally generated radiation. Because of the optical feedback, lasing and stimulated Raman scattering (SRS) have been observed from liquid droplets with astonishingly low pump intensity thresholds. Color photographs show that the radiation of lasing droplets and of droplets undergoing SRS is confined just inside the liquid-air interface where the optical feedback is high. (See publications #2 and #3 for color photographs.)

The lasing spectra were noted to consist of sharp peaks within the broad fluorescence wavelength region. These lasing peaks are separated by nearly equal wavelengths,

in accordance with the MDR's of a sphere with large X and with the index of refraction m > 1. Small changes in the lasing peaks have been used as indicators of small radius changes resulting from the evaporation of each droplet within the linear stream of flowing droplets. In addition, utilizing the small amount of wavelength oscillation in these peaks, we have deduced the amount of small shape oscillation. From the frequency and the damping rate of the oscillation amplitudes, we can extract the dynamic surface tension and the bulk viscosity of the droplet. (See publication #4 for a summary of this diagnostic technique.)

The SRS spectra can be used to provide information on the molecular species contained within the droplet and, to a lesser extent, information on the species concentration. The energy loss of the SRS peaks (usually measured in wave number shifts from the input laser radiation) is equal to the molecular vibrational energy. Thus, the wave number locations of the SRS peaks are fingerprints of the molecular species contained within the droplet. The intensity of the SRS peaks has been shown to monotonically increase with species concentration. However, fluctuations in the SRS peak intensity are large and, therefore, the SRS intensity is not an accurate measure of species concentration. (For more details on the use of SRS for species identification, see publication #5.)

In addition to lasing and SRS, three additional nonlinear optical effects were observed in large X and transparent droplets. One such nonlinear effect is multiorder Raman scattering which can be readily seen from liquid droplets. The second-order SRS can be pumped by the internal fields of the incident radiation and the first-order SRS. The third-order SRS can be pumped by the internal field of the second-order SRS. With such successive pumping by the first-order SRS process, up to the 14th-order SRS has been observed (see publication #6).

The second nonlinear optical effect observed from large X and transparent droplets is phase-modulation broadening of the elastically scattered radiation and of the SRS.

Because the internal radiation at λ_0 and at the multiorder SRS wavelengths is so intense, the refractive index of the droplet is altered, i.e., m changes from m_0 at low intensity to $m_0 + n_2 I(t)$ at high intensity, where n_2 is commonly referred to as the intensity-dependent index of refraction. Since the refractive index is proportional to the time-varying intensity I(t), the internal waves circumventing the droplet-air interface experience a time-varying phase shift and, hence, a frequency modulation. Using a time-averaged detection system, the effect of frequency modulation is observed as a wavelength broadening of the scattered radiation originally centered at λ_0 and/or at the various multiorder SRS wavelengths (see publication #7).

Coherent Raman gain is the third nonlinear optical effect observed from large X and transparent droplets which are irradiated by two input beams with wavelengths at λ_0 and λ_1. The second beam provides additional Raman gain and parametric signals at the first-order Stokes of the first beam. The combined effect of the additional gain and the parametric signals due to the presence of the second beam is to lower the SRS threshold of the first beam (see publication #8).

Several invitations to international conferences on nonlinear optics gave us the opportunity to review our findings on optical effects from single droplets. (See publications #9 - #12.)

LIB and Explosive Vaporization

Ethanol droplets containing efficient fluorescent molecules are known to reach the laser threshold at remarkably low input pump intensity. We investigated the emission properties of lasing droplets at input pump intensity levels far beyond the lasing thresholds. The following sequence of emission events occurs as a function of increasing pump intensity: (1) lasing emission is reached with low input intensity; (2) both SRS and laser emission are noted at higher input intensity; (3) the internal laser intensity is sufficient to induce SRS at still higher input intensity; and (4) the LIB threshold is reached when

the input pump intensity reaches ≈1 GW/cm^2, causing the appearance of an intense continuum emission associated with the recombination of the plasma and the deceleration of the electrons. Once the LIB threshold has been reached, the plasma emission is observed from not only within the droplet but also outside it in the region behind the illuminated face. Whereas the emission within the droplet consists of a broad continuum that extends toward the UV range, the emission outside the droplet consists of a broad continuum and discrete peak emission, which is characteristic of fluorescence from highly excited atomic and ionized species, such as singly ionized nitrogen N(II) and singly ionized oxygen O(II) in air. (For more details, see publication # 13.)

One of the key questions in the field of the LIB of transparent droplets with $X >> 1$ is the location of the breakdown initiation, i.e., is the breakdown initiated within the droplet shadow face where the internal intensity is concentrated or outside the droplet shadow face where the external intensity is even higher than the internal intensity? We modified our spectrograph in such a way that the spatial information along the vertical spectrograph slit is preserved. If a two-dimensional optical multichannel vidicon is placed at the exit plane of the spectrograph, this vidicon can detect both the spectral information dispersed along the horizontal direction and the spatial information preserved along the vertical direction. This instrument then enables us to determine simultaneously the plasma emission from many points (both within and outside the droplet) along an axis parallel to the laser beam. Our results indicate that LIB is initiated outside the shadow face for water droplets surrounded by a low LIB threshold gas such as Ar. However, LIB is initiated inside the shadow face for water droplets (radius < 40 μm) surrounded by air. In the case of larger water droplets (radius > 50 μm) surrounded by air, the location of LIB initiation shifts to the region outside the shadow face. For fluorocarbon (C_8F_{18}) liquid, known for its high dielectric breakdown strength, the LIB of C_8F_{18} droplets is always initiated in the gas region outside the droplet shadow face. For more details, see publications # 14 and # 15.

Another key question in field of the LIB of transparent droplets relates to the electron density and species temperature within different parts of the plasma plumes that are ejected from the droplet interface. We used the spatial preserving spectrograph-vidicon instrument described above to determine the plasma emission line shape along a line parallel to the laser beam. The spectral linewidth of discrete emission peaks from atomic species is known to be broadened by the electric fields of the electrons surrounding the atomic species, i.e., atomic line broadening results from the electric fields of the electrons through the first- or second-order Stark effect. We were, therefore, able to extract the spatial variation of the electron density along a line by noting the linewidth broadening of the atomic emission peak along a line which encompasses the regions outside the droplet illuminated and shadow faces. In addition to a density variation, an asymmetry in the electron density is noted in these two regions. Based on the appearance of a line reversal in the line shape of the resonance emission from Na or Li markers placed in the water droplet in the form of NaCl or LiCl, we conclude that the region in front of the shadow face is optically thicker than the region behind the illuminated face. The intensity ratio of two discrete wavelength peaks of the same species can be used as an indicator of the species temperature, provided that local thermodynamic equilibrium has been reached within the plasma plume. We measured the intensity ratio of the hydrogen Balmer lines and were able to extract the hydrogen temperature along a line which encompasses the regions outside the droplet illuminated and shadow faces. For more details, see publication # 16.

The spectroscopic instrument used to determine the location of the LIB initiation, the electron density, and the atomic species temperature had spatial resolution but lacked temporal resolution. Through the DoD-University Research Instrumentation Program, we obtained a streak camera that has a time resolution in the 0.1 nsec range. We measured the propagation velocity of the plasma emission front by imaging a line, which encompasses the region within the droplet and the regions outside the droplet

illuminated and shadow faces, on the vertical slit of the streak camera. Using this technique, we also determined the propagation velocity of the plasma emission for the following: (1) the plasma ejected from the droplet shadow face; (2) the plasma traveling inside the droplet from the shadow face toward the illuminated face; (3) with the laser pulse on, the plasma ejected from the illuminated face after the internal plasma has reached the illuminated face; and (4) with the laser pulse off, the external plasma traveling toward the laser from the droplet illuminated face. At high input intensites, the propagation velocities of the plasma traveling toward the laser provide information on the optical detonation wave. The response of our streak camera is not fast enough for us to determine the velocity of the breakdown wave that is initiated just outside the droplet shadow face during the rising portion of the laser pulse. (For more details, see publication #17.)

A transparent droplet is transformed into an absorbing droplet once LIB occurs. The plasma produced by the LIB process during the initial part of the laser pulse can absorb and scatter the remaining part of the incident radiation. Once LIB is initiated within the droplet shadow face region, the absorbed laser energy is subsequently localized in this region. This localized absorption eventually heats the entire droplet via the thermal diffusive mechanism which takes several milliseconds for micrometer-size droplets. The DoD-University Research Instrumentation Program also provided us with a framing camera that is capable of photographing a droplet every 50 nsec with a frame time of 10 nsec. Using a back-illuminated technique, we photographed a transparent water droplet at various time delays after irradiation by a green high intensity laser beam (λ_0 = 0.532 μm). Such ultrafast photographs reveal that vapor first emerges from the droplet shadow face and that the shadow face is partially consumed by the vaporization process. At a subsequent time, long after the laser pulse is shut off, more and more of the droplet shadow face is consumed as the heat travels from the shadow face toward the illuminated face. We were able to measure the ejected vapor velocity, the

receding velocity of the liquid-air interface starting from the shadow face side, and the velocity of the remaining droplet as it is propelled toward the laser by the rapid vaporization occurring at the shadow face. (For more details on the fate of the transparent droplet after LIB has been initiated, see publication # 18.)

Similar ultrafast photographs were taken with the framing camera of an absorbing water droplet and of a partially absorbing ethanol droplet after irradiation by a CO_2 laser pulse (λ_0 = 10.6 μm). For a water droplet, the absorption coefficient at 10.6 μm is so large that the CO_2 radiation is absorbed within a crescent-shaped region at the illuminated face. After the laser pulse is shut off, rapid vaporization occurs at the illuminated face, and the remaining water droplet is propelled away from the laser. A part of the illuminated face is consumed by the rapid vaporization, and the liquid-air interface starts to recede from the illuminated face and continues to recede toward the shadow face. The absorption coefficient of an ethanol droplet at 10.6 μm is not as large as that of water. Due to the focusing effect of the spherical illuminated face, the CO_2 radiation is concentrated toward the ethanol droplet shadow face and, therefore, the absorption is localized in this high intensity region. Rapid vaporization starts at the shadow face, and the remaining droplet is propelled toward the laser. More and more of the shadow face is removed as the rapid vaporization continues. The liquid-air interface starts to recede from the shadow face and continues to recede toward the illuminated face. It is interesting to compare the photographs of the transparent water droplet after irradiation by a green laser beam, the highly absorbing water droplet after irradiation by a CO_2 laser beam, and the moderately absorbing ethanol droplet after irradiation by a CO_2 laser beam. Whether the laser energy is initially absorbed by the molecular vibrations (e.g., water and ethanol droplets at λ_0 = 10.6 μm) or by the plasma resulting from the LIB (e.g., water droplets at λ_0 = 0.532μm) does not seem to affect the fate of the droplet after the laser pulse ends. For more details, see publication # 19.

A request to contribute a paper for a special issue of Applied Optics devoted to propagation and scattering in the atmosphere gave us a chance to review our work in the field of LIB in transparent liquid droplets. (For details, see publication #20.)

Multiple Scattering

Experimental data on multiple scattering from well characterized micrometer-size objects provide important test cases for modelers engaged in developing complicated computer codes for multiple scattering from an ensemble of aerosols. Our objective was to investigate the multiple scattering of two interfering and interacting fibers, using the fiber-mirror configuration as a prototype experiment for the more complicated two-fiber experiment.

Our experimental fiber-mirror configuration was dictated by the major difficulty in maintaining parallelism between the two fibers while changing their separation distance. However, it was not difficult to maintain a parallel alignment between the mirror surface and the fiber axis as the fiber-mirror distance d was varied. Using an optically flat mirror ensures that the image fiber has the same radius as the actual fiber (≈ 5 μm) which is held stationary in front of the movable mirror. The front surface of an Au or Ag mirror was mounted on a piezoelectric translator which was ramped by a periodic sawtooth waveform. The fiber-mirror combination was illuminated by a broadband tungsten light source, and the scattered radiation was dispersed by a spectrograph and detected by an intensified linear array detector. Consequently, the scattered radiation over a large wavelength region was simultaneously detected as d was linearly ramped.

Typical scattering spectra from the fiber-mirror combination consist of peaks at wavelengths that correspond to MDR's. When $d \gg a$, interference effects from the actual and image fibers are observed. However, when $d \approx a$, both interference and interacting effects are noted in the scattered spectra. The scattering spectra become particularly interesting when $d < a$. For the TE case, the perpendicular component of the scattered

fields (relative to the mirror surface) can excite the surface plasmons associated with the Au or Ag mirror. In the TM case, the surface plasmons play a lesser role, and the two interacting fibers play the dominant role since the surface plasmons cannot be excited with a tangential electric field (relative to the mirror surface). We noted that, when $d \approx a$, the fiber-mirror interaction causes the locations of the MDR's to be shifted away from those with $d >> a$. Such shifting in the MDR's was confirmed by a computer calculation based on the exact solution for the scattering spectrum of two interacting fibers. These exact calculations were made feasible by the close collaboration with Prof. Peter W. Barber of Clarkson University. The agreement between the experiment of the fiber-mirror configuration of two identical fibers was remarkable. Our results further the basic understanding of light scattering from two closely spaced particles which are larger in size than the incident wavelengths. (For more details about our results on the calculations of two fibers and on the fiber-mirror experiments, see publication #21.)

PUBLICATIONS RESULTING FROM THE RESEARCH

Nonlinear Optical Effects

1. D.S. Benincasa, P.W. Barber, J.-Z. Zhang, W.-F. Hsieh, and R.K. Chang, "Spatial Distribution of the Internal and Near-Field Intensities of Large Cylindrical and Spherical Scatterers," Appl. Opt. 26, 1348 (1987).

2. S.-X. Qian, J.B. Snow, H.-M. Tzeng, and R.K. Chang, "Lasing Droplets: Highlighting the Liquid-Air Interface by Laser Emission," Science 231, 486 (1986).

3. J.B. Snow, S.-X. Qian, and R.K. Chang, "Nonlinear Optics with a Micrometer-Size Droplet," Opt. News 12 (5), 5 (1986).

4. H.-M. Tzeng, M.B. Long, R.K. Chang, and P.W. Barber, "Size and Shape Variations of Liquid Droplets Deduced from Morphology-Dependent Resonances in Fluorescence Spectra," in Proceedings of the SPIE Particle Sizing and Spray Analysis Conference, Vol. 573 (SPIE, Bellingham, Washington, 1985), p. 80.

5. J.H. Eickmans, S.-X. Qian, and R.K. Chang, "Detection of Water Droplet Size and Anion Species by Nonlinear Optical Scattering," Part. Charact. 4, 85 (1987).

6. S.-X. Qian and R.K. Chang, "Multiorder Stokes Emission from Micrometer-Size Droplets," Phys. Rev. Lett. 56, 926 (1986).

7. S.-X. Qian and R.K. Chang, "Phase-Modulation-Broadened Line Shapes from Micrometer-Size CS_2 Droplets," Opt. Lett. 11, 371 (1986).

8. S.-X. Qian, J.B. Snow, and R.K. Chang, "Coherent Raman Mixing and Coherent Anti-Stokes Raman Scattering from Individual Micrometer-Size Droplets," Opt. Lett. 10, 499 (1985).

9. S.-X. Qian, J.B. Snow, and R.K. Chang, "Nonlinear Optical Processes in Micron-Size Droplets," in Laser Spectroscopy VII, T.W. Hänsch and Y.R. Shen, eds. (Springer-Verlag, Berlin, 1985), p. 204.

10. R.K. Chang, S.-X. Qian, and J. Eickmans, "Stimulated Raman Scattering, Phase Modulation, and Coherent Anti-Stokes Raman Scattering from Single Micrometer-Size Liquid Droplets," in Methods of Laser Spectroscopy, Y. Prior, A. Ben-Reuven, and M. Rosenbluh, eds. (Plenum Press, New York, 1986), p. 249.

11. R.K. Chang, "Micrometer-Size Droplets as Optical Cavities: Lasing and Other Nonlinear Effects," in Advances in Laser Science-II, M. Lapp, W.C. Stwalley, and G. A. Kenney-Wallace, eds. (American Institute of Physics, New York, 1987), p. 509.

12. R.K. Chang, "Nonlinear Optical Phenonema in Single Micron-Size Droplets," in Laser Optics of Condensed Matter, J.L. Birman, H.Z. Cummins, and A.A. Kaplyanski, eds. (Plenum Press, New York, 1988) p. 193.

LIB and Explosive Vaporization

13. W.-F. Hsieh, H.-M. Tzeng, and R.K. Chang, "High Intensity Laser Interactions with Micrometer-Size Dye Droplets," in Special Issue of the Annual Report of the Institute of Physics, Academia Sinica (Taiwan), Vol. 16, 1986, p. 1.

14. W.-F. Hsieh, J.H. Eickmans, and R.K. Chang, "Internal and External Laser-Induced Avalanche Breakdown of Single Droplets in an Argon Atmosphere," J. Opt. Soc. Am. B 4, 1816 (1987).

15. J.H. Eickmans, W.-F. Hsieh, and R.K. Chang, "Laser-Induced Explosion of H_2O Droplets: Spatially Resolved Spectra," Opt. Lett. 12, 22 (1987).

16. J.H. Eickmans, W.-F. Hsieh, and R.K. Chang, "Plasma Spectroscopy of H, Li, and Na in Plumes Resulting from Laser-Induced Droplet Explosion," Appl. Opt. 26, 3721 (1987).

17. W.-F. Hsieh, J.-B. Zheng, C.F. Wood, B.T. Chu, and R.K. Chang, "Propagation Velocities of Laser-Induced Plasma inside and outside a Transparent Droplet," Opt. Lett. 12, 576 (1987).

18. J.-Z. Zhang, J.K. Lam, C.F. Wood, B.T. Chu, and R.K. Chang, "Explosive Vaporization of a Large Transparent Droplet Irradiated by a High Intensity Laser," Appl. Opt. 26, 4731 (1987).

19. C.F. Wood, D.H. Leach, J.-Z. Zhang, R.K. Chang, and P.W. Barber, "Time-Resolved Shadowgraphs of Large Individual Water and Ethanol Droplets Vaporized by a Pulsed CO_2 Laser," Appl. Opt., in press.

20. R.K. Chang, J. Eickmans, W.-F. Hsieh, C.F. Wood, J.-Z. Zhang, and J.-B. Zheng, "Laser-Induced Breakdown in Large Transparent Water Droplets," Appl. Opt., in press.

Multiple Scattering

21. B. Schlicht, K.F. Wall, R.K. Chang, and P.W. Barber, "Light Scattering by Two Parallel Glass Fibers," J. Opt. Soc. Am. A 4, 800 (1987).

SCIENTIFIC COLLABORATORS

In addition to the principal investigator, the following people have participated in this project:

Theorists:	Peter W. Barber, Clarkson University
	Boa-Teh Chu, Yale University
Postdoctoral Associates:	Shu-chi Chen
	Johannes H. Eickmans
	Carol F. Wood
	Jia-biao Zheng
Senior Research Associate:	Stanley Mroczkowski
Graduate Students:	Wen-Feng Hsieh
	Jian-Zhi Zhang

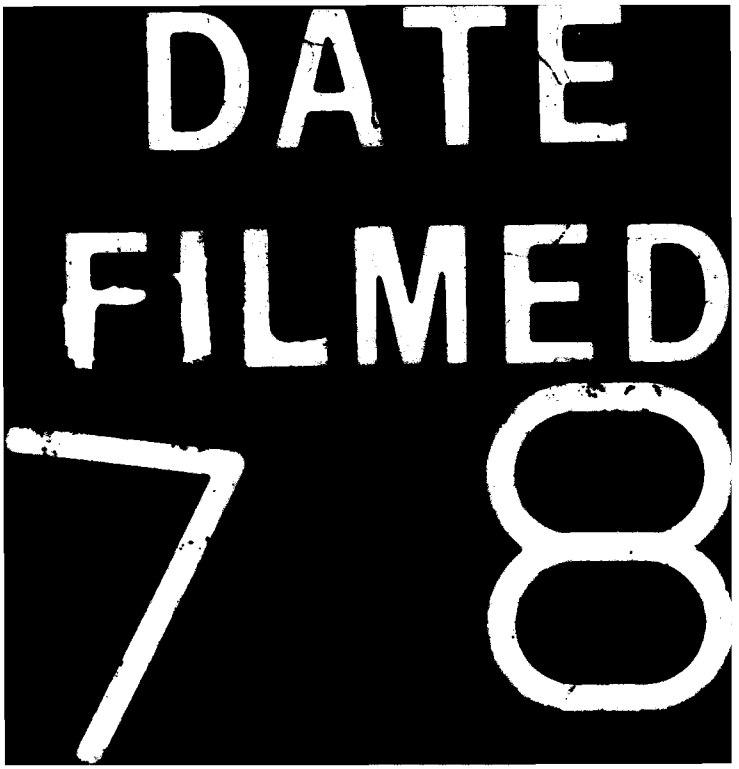
DATE
FILMED
7 8